Discovery of selective diacylglycerol lipase β inhibitors

Zhu, N.

Chapter 6

Glycine sulfonamides act as selective DAGLβ inhibitors and reduce inflammation

6.1 Introduction

Lipids, such as endocannabinoids[1–4], diacylglycerols[5], eicosanoids[6] and fatty acids[7], have been recognized as signaling molecules that regulate important physiological processes, including neurotransmission, metabolism, cell proliferation and immune response. Distinct from classical chemical messengers stored in vesicles, signaling lipids are produced 'on demand' and rapidly inactivated to terminate their actions.[8] For instance, endocannabinoid 2-arachidonoylglycerol (2-AG) is produced by diacylglycerol lipase α and β (DAGLα and DAGLβ)[9] and degraded by monoacylglycerol lipase (MAGL) and α/β-hydrolase domain-containing 6/12 (ABHD6/12)[10,11] after action. DAGLs regulate diacylglycerols and 2-AG via direct substrate-product relationships. Additionally, they also exert effects indirectly on other bioactive lipids, such as arachidonic acid (AA) and prostaglandins E2 and D2 (PGE_2 and PGD_2), through interconnecting enzymes such as MAGL and cyclooxygenase (COX). These lipids occupy the hubs of distinct but integrated signaling pathways[3,6,12–16] to form a sophisticated lipid crosstalk which affects physiological and pathological processes in a complex and dynamic manner.[14,17]

DAGL enzymes are transmembrane serine hydrolases which employ the classical Ser-His-Asp catalytic triad to specifically hydrolyze the *sn*1 ester bond of diacylglycerols.[9] Genetic studies with constitutive disruption of DAGLα or DAGLβ have confirmed that they contribute differently to the production of 2-AG in various cell and tissue types.[18–20] In general, DAGLα is the dominant regulator of bulk of 2-AG biosynthesis in the brain, whereas DAGLβ is the principal 2-AG biosynthetic enzyme in periphery[18,21] and in immune-related cells.[20,22] Genetic disruption[18] and pharmacological inhibition[23] of DAGLα were found to rewire brain lipid signaling networks, which negatively impacted emotional states such as fear extinction, stress and anxiety.[24,25] By contrast, DAGLβ disruption exerted potentially therapeutic effects related to microglia and macrophage function, by reducing lipopolysaccharide (LPS)-induced inflammation without significant alternations of total brain levels of 2-AG.[20]

In Chapter 4, a series of glycine sulfonamides were discovered as DAGLβ selective inhibitors. Based on their high potency and selectivity over DAGLα, six inhibitors (Figure 6.1) were selected for further profiling in this Chapter. In addition, a negative control compound was generated which is structurally similar to the glycine sulfonamides but inactive against DAGLβ. The results presented in this Chapter reveal that LEI-130 and LEI-131 represent compounds with the most optimal properties. They behave as noncompetitive DAGLβ inhibitors with high selectivity over other serine hydrolases and other proteins in the endocannabinoid system. Moreover, LEI-130 and LEI-131 targeted endogenous DAGLβ and impacted diverse signaling lipid networks depending on the cell type. These findings, taken together, demonstrate that LEI-130 and LEI-131 are potent, selective and cellularly active DAGLβ inhibitors which could lead to potential treatments of inflammation and other disorders.

6.2 Results

6.2.1 LEI-130 and LEI-131 are potent and selective DAGLβ inhibitors

In Chapter 4, six glycine sulfonamides (**1-6**), based on initial screening hit LEI-106, were discovered as selective DAGLβ inhibitors using EnzChek lipase substrate assays (Figure 6.1). The compounds share notable structural similarities, featuring a glycine sulfonamide core structure (red), a substituted benzylamine (black), and a 3,4-dihydro-2*H*-benzo[*b*][1,4]dioxepine (blue) on the sulfonyl substituent. These inhibitors exhibited high potency (pIC_{50} > 7.4) and good selectivity (> 35-fold) for DAGLβ with low lipophilicity (cLogD < 3) and high lipophilic efficiency (LipE > 5) (Table 6.1 and see also Chapter 4). To assess DAGLβ involvement in biological studies, a negative control compound (**7**, **LEI-132**) lacking DAGL inhibitory activity was generated.

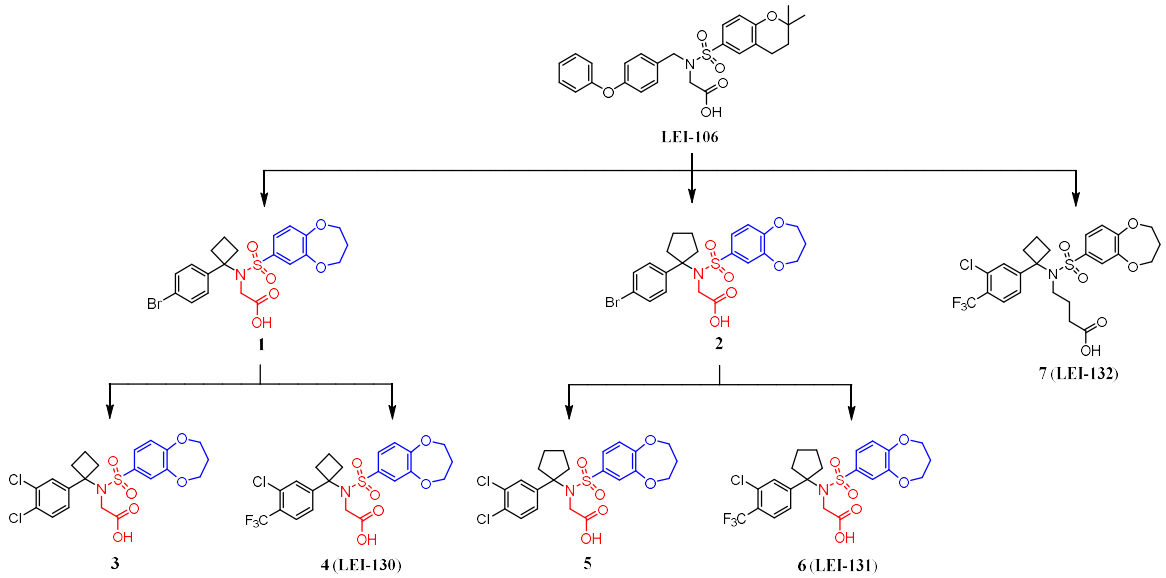

Figure 6.1 Discovery of DAGLβ inhibitors **1-6** and an inactive control **7** starting from hit LEI-106.

Table 6.1 Biochemical results, ABPP results, and physiochemical properties of compounds **1-7**.[a]

ID	Biochemical pIC_{50} DAGLβ	Apparent biochemical selectivity	ABPP pIC_{50} DAGLβ	Apparent ABPP selectivity	MW (Da)	cLogD	tPSA (Å²)	Biochemical LipE DAGLβ	ABPP LipE DAGLβ
1	7.48 ± 0.09	35	7.46 ± 0.09	39	496.37	1.4	104	6.1	6.1
2	8.08 ± 0.13	37	8.19 ± 0.06	37	510.40	1.8	104	6.3	6.4
3	7.88 ± 0.09	41	8.12 ± 0.12	35	486.36	1.9	104	6.0	6.2
4 (LEI-130)	7.94 ± 0.08	40	7.89 ± 0.11	36	519.92	2.2	104	5.7	5.7
5	8.07 ± 0.09	51	8.20 ± 0.08	19	500.38	2.3	104	5.8	5.9
6 (LEI-131)	7.96 ± 0.06	39	8.54 ± 0.11	76	533.94	2.5	104	5.5	6.0
7 (LEI-132)	< 5	-	-	-	547.97	3.1	104	-	-

[a]The negative logarithm of the half-maximal inhibitory concentration (pIC_{50}) was determined using EnzChek lipase substrate assay (biochemical) and activity-based protein profiling (ABPP). Molecular weight (MW), the calculated logarithm of the *n*-octanol-water partition coefficient at pH 7.4 (cLogD) and the topological polar surface area (tPSA) were calculated using DataWarrior 5.0.0. Lipophilic efficiency (LipE) was computed using the formula LipE = pIC_{50} – cLogD.

Here, the DAGL-tailored activity-based probe, DH379 (Figure 6.2B), was employed in activity-based protein profiling (ABPP) as a complementary, orthogonal assay to evaluate the activity and selectivity of inhibitors **1-6** on recombinant human DAGLβ and DAGLα. DH379 effectively labeled DAGL enzymes and pre-incubation with inhibitors **1-6** concentration dependently blocked the labeling of DAGL (Figure 6.2A). The quantification of the fluorescent signals generated concentration-response curves as depicted in Figure 6.2C. These compounds demonstrated high potency and selectivity for DAGLβ over DAGLα in ABPP assays (Table 6.1), aligning with the results observed in DAGL EnzChek lipase substrate assays in Chapter 4. Among these inhibitors, compound **6** exhibited the highest activity and selectivity for DAGLβ with a pIC_{50} of 8.54 ± 0.11 and a 76-fold selectivity. Compound **5** had a pIC_{50} of 8.20 ± 0.08 for DAGLβ but only a 19-fold selectivity in the ABPP assay, significantly lower compared to the biochemical assay. Compound **1** showed the lowest activity (pIC_{50} of 7.46 ± 0.09) for DAGLβ. Compounds **2**, **3** and **4** displayed high potency and moderate selectivity for DAGLβ (~35-fold). Among them, compound **4** belongs the cyclobutyl series and is most structurally similar to compound **6** and the negative control **7**. Taken together, inhibitors **4** (**LEI-130**) and **6** (**LEI-131**) were selected for further biological profiling.

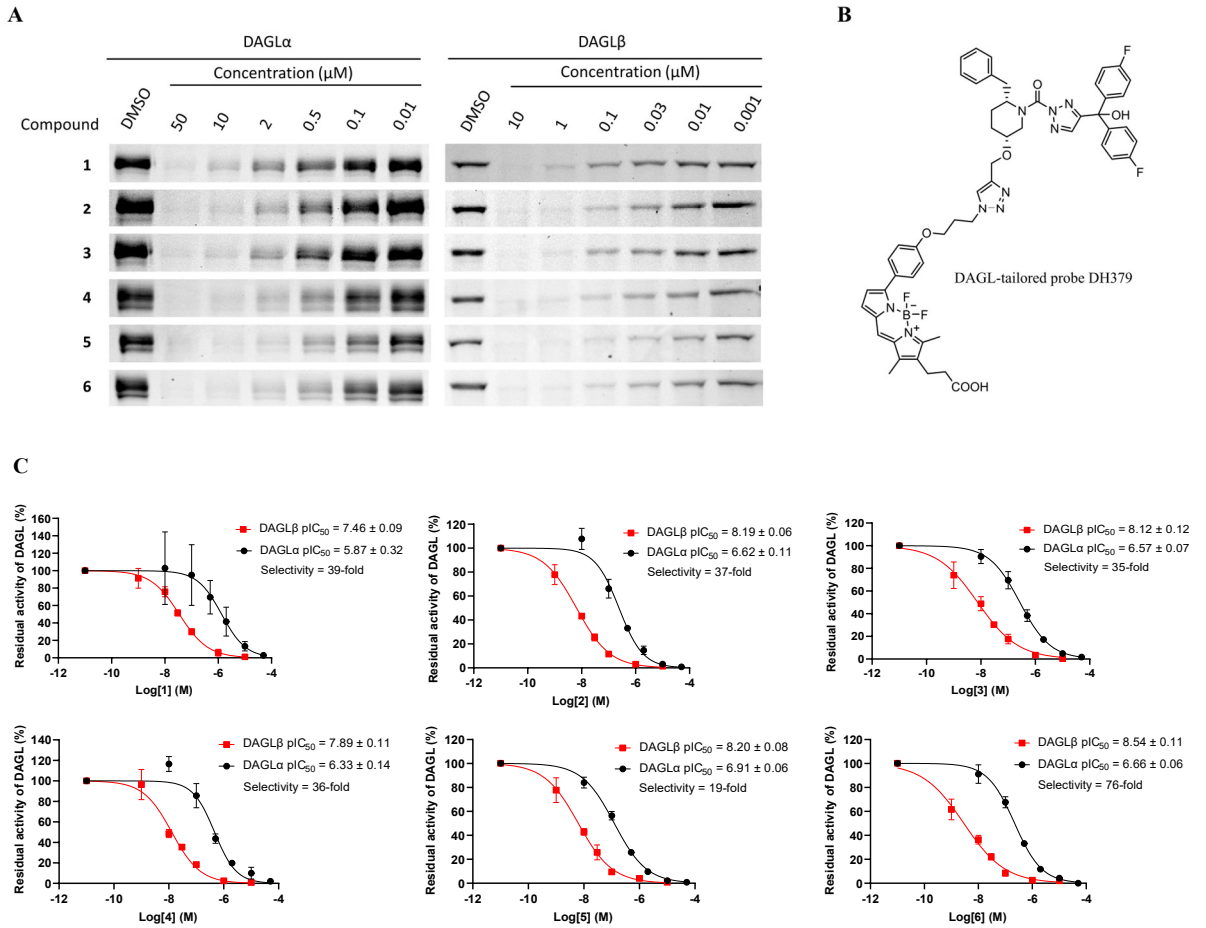

Figure 6.2 *In vitro* activity of compounds **1-6** on recombinant human DAGLα and DAGLβ. (A) Representative gel excerpts of ABPP experiments with compounds **1-6** on recombinant human DAGLα and DAGLβ using probe DH379 (0.5 μM, 10 min). (B) Chemical structure of probe DH379. (C) Concentration-response curves as well as pIC_{50} and selectivity values of inhibitors **1-6**. Data shown are mean ± SD (n = 1, N = 3).

6.2.2 LEI-130 and LEI-131 demonstrate a noncompetitive inhibition mode for DAGLβ

To investigate the inhibition mode of glycine sulfonamides LEI-106, LEI-130 and LEI-131, Michaelis-Menten kinetic assays were performed (Figure 6.3A-C). The kinetic analysis revealed a significant decrease in the maximum rate (V_{max}) with an increase in inhibitor concentration, but the Michaelis constant (K_M) remained relatively stable within the range of 0.24 to 0.31 µM (Supplementary Table S6.1), suggesting these compounds do not inhibit DAGLβ via a competitive mechanism. Lineweaver Burk analysis further demonstrated that LEI-106 inhibited DAGLβ via an uncompetitive inhibition mode (Figure 6.3D), while LEI-130 and LEI-131 exhibited a noncompetitive behaviour (Figure 6.3E, F). Of interest, LEI-106, LEI-130 and LEI-131 displayed an uncompetitive inhibition mode for DAGLα (Supplementary Figure S6.1 and Table S6.2). After determining the inhibition mode, the inhibition constant (K_i) and selectivity could be calculated (Table 6.2). LEI-130 and LEI-131 exhibited a pK_i of 7.94 ± 0.08 and 7.96 ± 0.06 for DAGLβ, respectively, with a 22-fold selectivity.

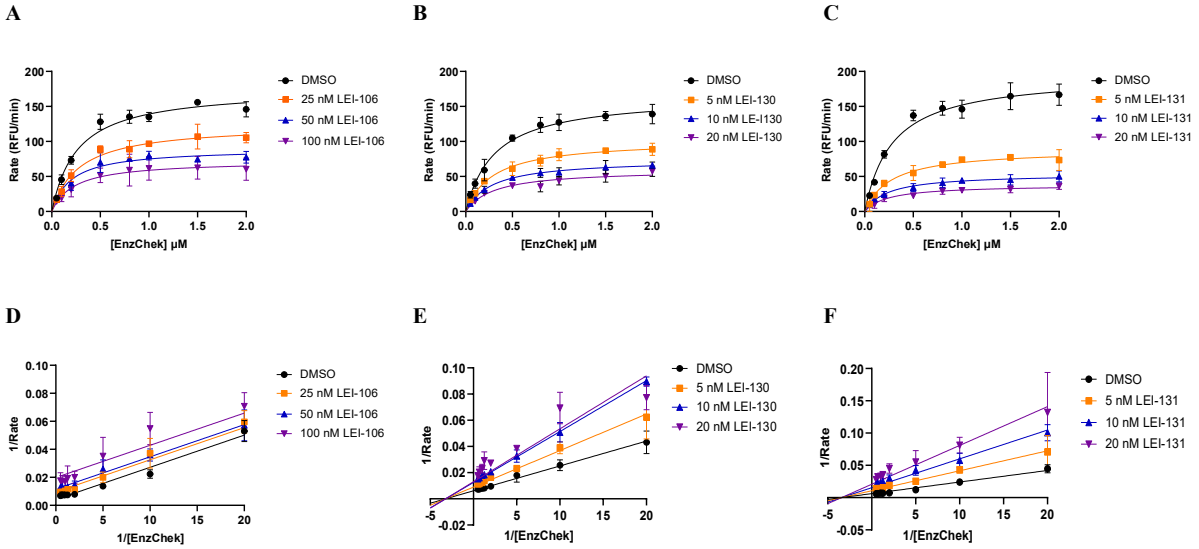

Figure 6.3 Mode-of-inhibition studies of LEI-106, LEI-130 and LEI-131 against DAGLβ. (A-C) Michaelis-Menten kinetic curves. Rate of EnzChek hydrolysis by DAGLβ as a function of substrate concentration in the presence of different concentrations of LEI-106, LEI-130 and LEI-131. (D-F) Lineweaver Burk plots. Data shown are mean ± SD (n = 2, N = 2).

Table 6.2 Biochemical activity, inhibition mode, inhibition constant and selectivity of LEI-106, LEI-130 and LEI131.[a]

Compound	pIC_{50} DAGLα	Inhibition mode DAGLα	pIC_{50} DAGLβ	Inhibition mode DAGLβ	pK_i DAGLα	pK_i DAGLβ	Selectivity DAGLβ
LEI-106	7.35 ± 0.06	uncompetitive	6.69 ± 0.14	uncompetitive	7.60 ± 0.06	6.87 ± 0.14	0.2
LEI-130	6.34 ± 0.09	uncompetitive	7.94 ± 0.08	noncompetitive	6.59 ± 0.09	7.94 ± 0.08	22
LEI-131	6.37 ± 0.05	uncompetitive	7.96 ± 0.06	noncompetitive	6.62 ± 0.05	7.96 ± 0.06	22

[a]The negative logarithm of the inhibition constant (pK_i) was computed using formula $pK_i = pIC_{50} + \log_{10}(1 + K_M/[S])$ and $pK_i = pIC_{50}$ for uncompetitive and noncompetitive inhibitors, respectively. The Michaelis constants (K_M) were 0.39 µM and 0.26 µM for DAGLα and DAGLβ, respectively. Substrate concentration ([S]) was 0.5 µM.

6.2.3 LEI-130 and LEI-131 are selective over other serine hydrolases and proteins in the endocannabinoid system

To assess the selectivity of DAGLβ inhibitors LEI-130 and LEI-131 and the control compound LEI-132 over a panel of serine hydrolases, gel-based competitive ABPP was conducted. This involved pre-incubating the compounds with mouse brain membrane or cytosol proteome, followed by sequential labeling the serine hydrolases using broad-spectrum probes MB064 and FP-BODIPY. As shown in Figure 6.4A, MB064 labeled endogenous DAGLα in mouse brain membrane proteome along with other serine hydrolases such as ABHD6, ABHD12, and ABHD16A. MB064 also labeled a selection of serine hydrolases in the cytosol proteome. LEI-130, LEI-131 and LEI-132 showed no inhibition on these labeled proteins across a broad concentration range from 1 nM to 10 µM. However, LEI-106 at 10 µM completely blocked the labeling of DAGLα and two other bands (band 1 and 2), while enhancing the labeling of a protein (band 3) in both membrane and cytosol proteomes (Supplementary Figure S6.2A). FP-BODIPY labeled different serine hydrolases compared to MB064, such as fatty acid amide hydrolase (FAAH) and MAGL (Figure 6.4B). The labeling of these proteins remained unaffected by LEI-130, LEI-131 and LEI-132. These findings indicate that LEI-130 and LEI-131 are more selective than hit compound LEI-106 and they exhibit selectivity for DAGLβ without interfering with the activity of other serine hydrolases.

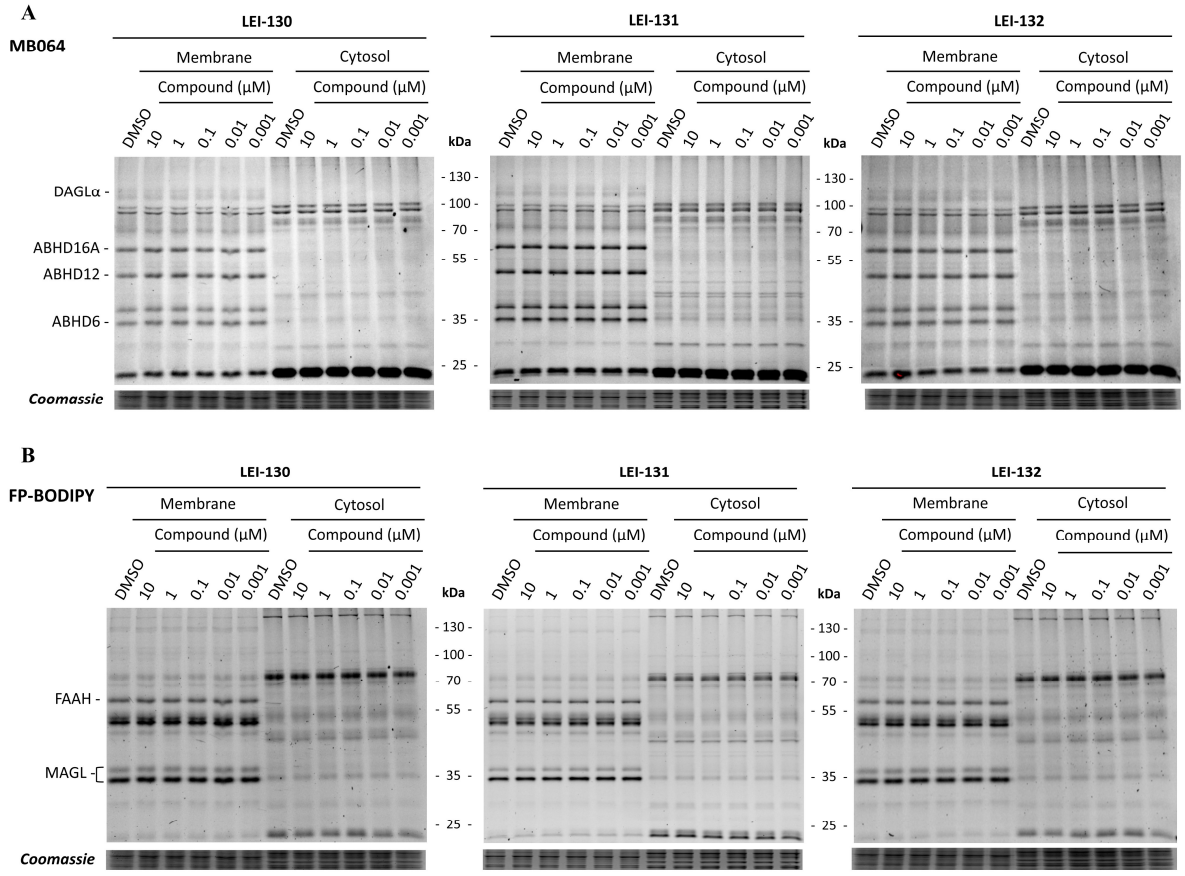

Figure 6.4 *In vitro* selectivity of LEI-130, LEI-131 and LEI-132 on mouse brain proteomes. Representative gels of ABPP experiments using MB064 (A, 250 nM, 10 min) and subsequently FP-BODIPY (B, 100 nM, 10 min).

Next, the selectivity of LEI-130, LEI-131 and LEI-132 over human ABHD6 and MAGL, *N*-acylphosphatidylethanolamine phospholipase D (NAPE-PLD) and cannabinoid CB_1 and CB_2 receptors was determined. These compounds were inactive against ABHD6, MAGL, NAPE-PLD, CB_1R and CB_2R (< 50% inhibition or displacement at 10 µM, Table 6.3). These findings, taken together, demonstrate that LEI-130 and LEI-131 are selective DAGLβ inhibitors and the inactive compound LEI-132 serves as a suitable control compound.

Table 6.3 Biochemical activities of LEI-130, LEI-131 and LEI-132 for representative ECS enzymes and CB receptors. Percentage (%) inhibition or displacement at 10 µM.

Compound	ABHD6	MAGL	NAPE-PLD	CB_1R	CB_2R
LEI-130	20.5 ± 2.3%	26.9 ± 1.7%	4.8 ± 1.1%	-1 ± 8%	-6 ± 16%
LEI-131	10.0 ± 0.4%	35.3 ± 0.7%	3.1 ± 2.2%	-1 ± 9%	-9 ± 9%
LEI-132	4.2 ± 0.8%	24.4 ± 2.1%	6.8 ± 2.2%	-15 ± 11%	1 ± 8%

6.2.4 LEI-130 and LEI-131 play distinct roles in microglia and macrophage

To investigate the cellular target engagement of LEI-130 and LEI-131, a gel-based ABPP experiment was performed. Briefly, N9 microglia or J774A.1 macrophage cells were treated with the inhibitors (10 µM) or vehicle (DMSO) before incubation with probe DH379 (1 µM). Subsequently, the cells were lysed and analyzed using gel-based ABPP. The control compound LEI-132 was included for comparison. Probe DH379 labeled endogenous DAGLβ at the expected molecular weight both in N9 microglia (Figure 6.5A) and J774A.1 macrophage (Figure 6.5B) in the samples treated with the vehicle control. The labeling of DAGLβ, but not other proteins, by DH379 was completely blocked by DAGLβ inhibitors LEI-130 and LEI-131, but not by control compound LEI-132.

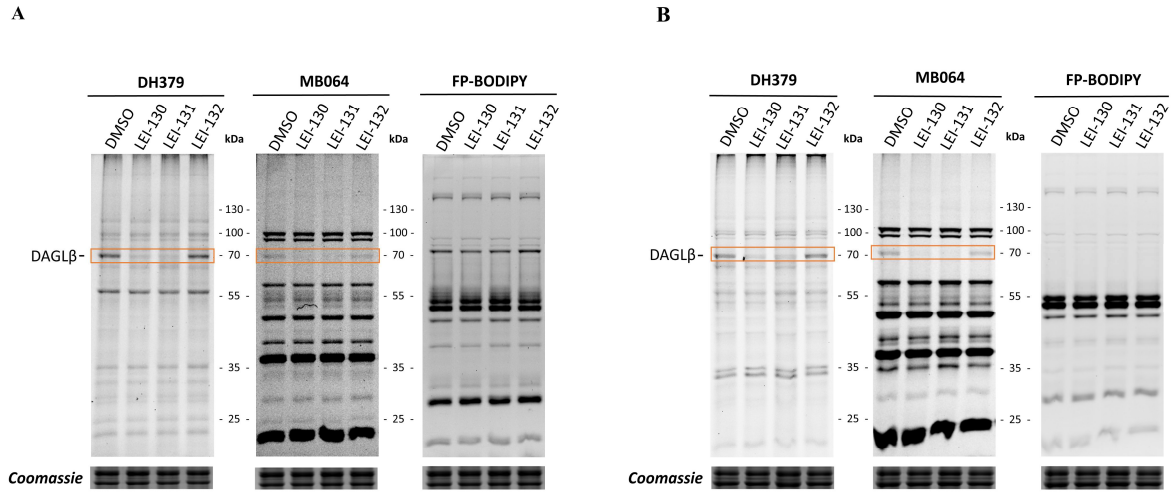

Figure 6.5 *In situ* target engagement and selectivity of LEI-130, LEI-131 and LEI-132. Representative gels of ABPP experiments with LEI-130, LEI-131 and LEI-132 (10 µM, 2 h) in N9 microglia (A) and J774A.1 macrophage (B) using DH379 (*in situ*, 1 µM, 1 h) or the cocktail of MB064 and FP-BODIPY (*in vitro*, 100 nM, 10 min).

Next, the cellular selectivity of LEI-130, LEI-131 and LEI-132 was assessed. N9 and J774A.1 cells were incubated with DMSO, LEI-130, LEI-131 or LEI-132 (10 μM) and subsequently lysed for analysis in gel-based ABPP using a cocktail of probes MB064 and FP-BODIPY (100 nM/each probe). This approach enabled simultaneous labeling of DAGLβ and a number of other serine hydrolases. In line, LEI-130 and LEI-131 efficiently inhibited endogenous DAGLβ without affecting other proteins. In contrast, control compound LEI-132 exhibited no inhibitory activity on any of the detected proteins, including DAGLβ. These findings collectively demonstrate that LEI-130 and LEI-131 are cell-permeable inhibitors capable of selectively targeting endogenous DAGLβ in microglia and macrophage cells.

Having established the cellular target engagement of DAGLβ by LEI-130 and LEI-131 in N9 microglia cells, it was investigated whether the compounds could modulate lipid networks in these cells. LEI-130 and LEI-131 (10 μM, 2 h) exhibited a significant reduction in 2-AG and a noticeable accumulation of 1-stearoyl-2-arachidonoyl-*sn*-glycerol (SAG) (Figure 6.6A, B). Conversely, a slight increase in 2-AG and no change in SAG were observed in LEI-132-treated cells. These results indicate that DAGLβ is the primary enzyme regulating the SAG and 2-AG levels in N9 microglia. Moreover, LEI-130 and LEI-131 significantly reduced the cellular levels of monoacylglycerols 2-linoleoylglycerol (2-LG) and 2-oleoylglycerol (2-OG), arachidonic acid (AA), PGE_2 and PGD_2, while sparing anandamide (AEA) (Figure 6.7C-H). Notably, these changes were also observed for the control compound LEI-132. These findings suggest the existence of other protein targets modulated by these compounds that regulate the levels of these lipids via DAGLβ-independent mechanisms in N9 microglia.

DAGLβ deletion protects primary microglia from lipopolysaccharide (LPS)-stimulated inflammation by reducing the production of proinflammatory cytokines.[20] To investigate the influence of acute DAGLβ inhibition on microglia inflammatory processes, N9 microglia cells were pre-treated with LEI-130, LEI-131 and LEI-132 (10 μM, 1 h) and stimulated with the proinflammatory agent LPS (5 ng/mL, 24 h), before analyzing the culture supernatants by the enzyme-linked immunosorbent assay (ELISA). LPS stimulation significantly elevated the levels of secreted interleukin-6 (IL-6) and tumor necrosis factor-α (TNF-α) (Figure 6.6I, J). The LPS-induced increase in IL-6 was significantly attenuated by both LEI-130 and LEI-131. However, there was only a modest, but significant, attenuation on LPS-induced secretion of TNF-α by LEI-131. Of note, LEI-132 also significantly reduced the LPS-induced production of IL-6 and TNF-α, suggesting that the cytokine production is not solely modulated by DAGLβ, but also by off-targets of these compounds.

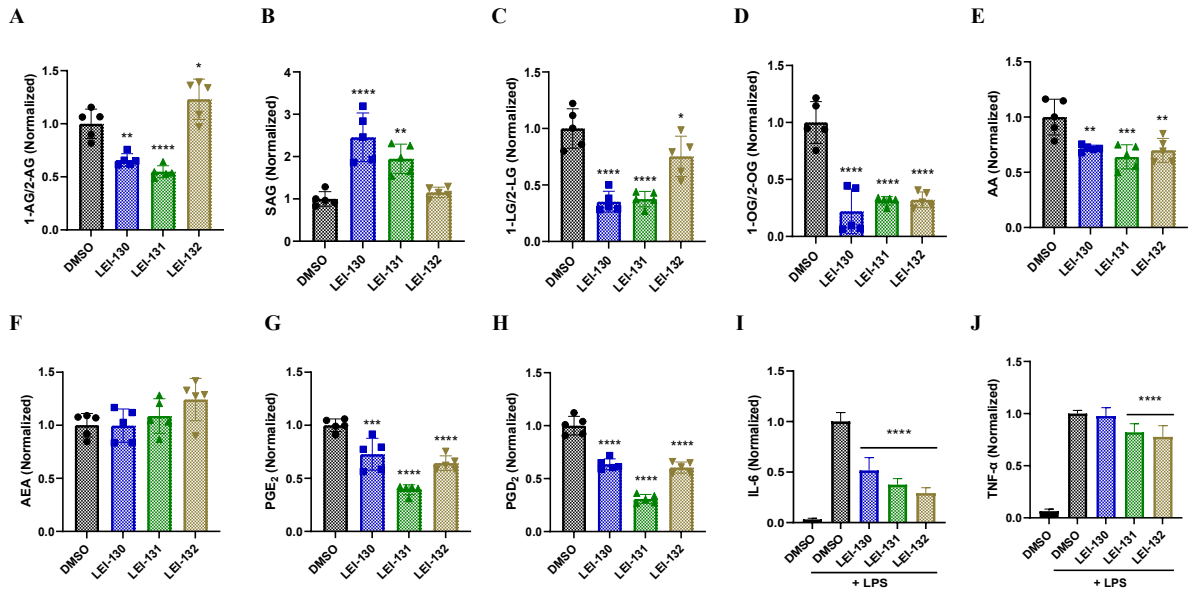

Figure 6.6 Relative levels of lipids and cytokines in N9 microglia. Normalized cellular levels of (A) 2-AG, (B) SAG, (C) 2-LG, (D) 2-OG, (E) AA, (F) AEA, (G) PGE_2, and (H) PGD_2 in N9 microglia cells treated with DMSO, LEI-130, LEI-131 and LEI-132 (10 μM, 2 h). Data shown are mean ± SD (n = 5). Normalized levels of (I) IL-6 and (J) TNF-α secreted by N9 microglia cells pre-treated with DMSO, LEI-130, LEI-131 and LEI-132 (10 μM, 1 h) upon LPS-stimulation (5 ng/mL, 24 h). Data shown are mean ± SD (n = 12-16). Statistical significance was calculated using one-way ANOVA. $^{*}P < 0.05$, $^{**}P < 0.01$, $^{***}P < 0.001$, $^{****}P < 0.0001$.

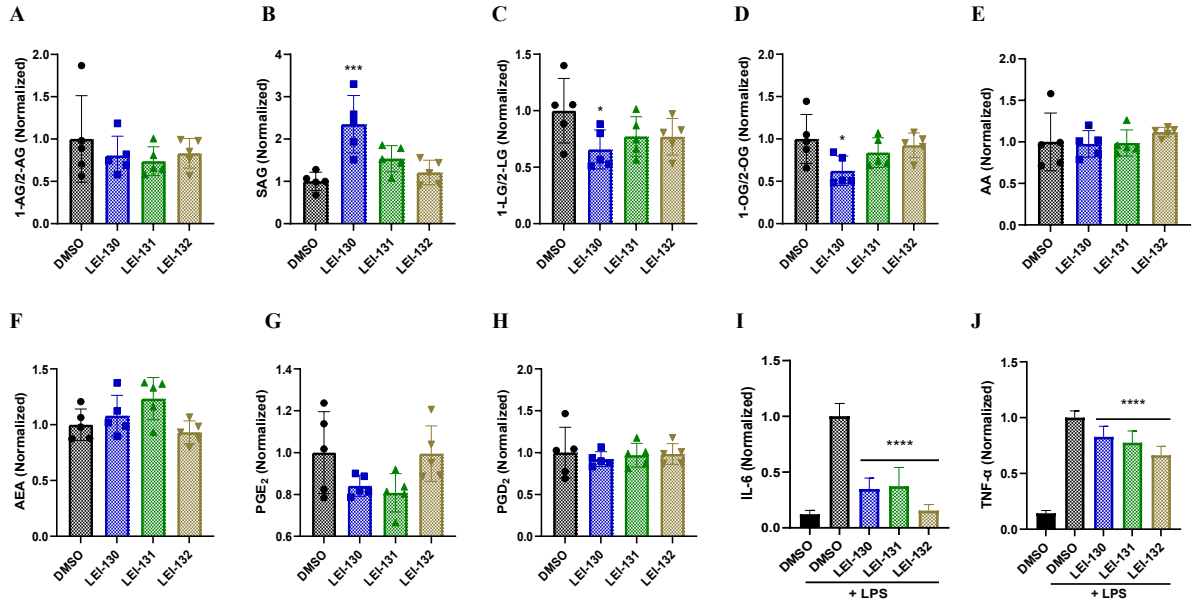

Figure 6.7 Relative levels of lipids and cytokines in J774A.1 macrophages. Normalized cellular levels of (A) 2-AG, (B) SAG, (C) 2-LG, (D) 2-OG, (E) AA, (F) AEA, (G) PGE_2, and (H) PGD_2 in J774A.1 macrophages treated with DMSO, LEI-130, LEI-131 and LEI-132 (10 μM, 2 h). Data shown are mean ± SD (n = 5). Normalized levels of (I) IL-6 and (J) TNF-α secreted by J774A.1 macrophages pre-treated with DMSO, LEI-130, LEI-131 and LEI-132 (10 μM, 1 h) upon LPS-stimulation (5 ng/mL, 24 h). Data shown are mean ± SD (n = 12-16). Statistical significance was calculated using one-way ANOVA. $^{*}P < 0.05$, $^{**}P < 0.01$, $^{***}P < 0.001$, $^{****}P < 0.0001$.

Lipidomics analysis and ELISA were also performed for J774A.1 macrophages. In contrast to the results observed in N9 microglia, treatment with LEI-130, LEI-131 and LEI-132 (10 μM, 2 h) in J774A.1 macrophages showed no significant changes in the levels of most bioactive lipids, including 2-AG, AEA, AA, PGE_2, and PGD_2 (Figure 6.7A, E-H). However, a significant accumulation of SAG and a modest reduction in 2-LG and 2-OG were observed in LEI-130-treated cells (Figure 6.7B-D). These results indicate that different metabolic pathways may exist that regulate 2-AG levels in J774A.1 macrophages. Despite their inability to reduce the levels of 2-AG, AA and prostaglandins, LEI-130, LEI-131, and LEI-132 displayed anti-inflammatory effects by significantly suppressing the LPS-stimulated production of proinflammatory cytokines IL-6 and TNF-α.

6.3 Discussion and conclusion

DAGLs play a central role in the lipid networks by integrating signaling pathways of various lipids, including DAG[16], endocannabinoids[3], AA and eicosanoids.[14] Benefitting from the discovery of *in vivo* active inhibitors[22,23], the biological functions of DAGLs have been gradually elucidated. However, understanding the specific roles of individual isoform, either DAGLα or DAGLβ, in biological processes has been challenging due to the lack of isoform-specific inhibitors. In an effort to address this problem, glycine sulfonamide DAGLβ-selective inhibitors LEI-130 and LEI-131 were developed and subjected to cellular studies.

Inhibitors can exert their effects on enzymes through specific ways, such as orthosteric and allosteric binding. A profound understanding of the interactions between inhibitors and enzymes is crucial for elucidating the regulatory mechanisms of enzymatic activity and discovering more specific inhibitors. Due to the absence of crystal structures for DAGL enzymes, our comprehension of these interactions between glycine sulfonamides and DAGL is limited. To address this, a homology model of DAGLα[26] was constructed and employed to understand the structure-activity relationship of glycine sulfonamide DAGL inhibitors.[27] It is important to note that this study initially hypothesized that glycine sulfonamides act as competitive inhibitors, occupying the orthosteric pocket. However, the mode-of-inhibition studies presented here contradict this hypothesis. Specifically, both LEI-130 and LEI-131 were identified as uncompetitive and noncompetitive inhibitors for DAGLα and DAGLβ, respectively, while LEI-106 was shown to be an uncompetitive inhibitor for both DAGL isoforms. This suggests that they occupy an allosteric pocket of DAGLs. During the optimization process, LEI-130 and LEI-131 exhibited increased selectivity and altered their mode of action for DAGLβ, but not for DAGLα. This indicates that the binding site of LEI-130 and LEI-131 in DAGLβ has undergone a slight shift compared to LEI-106, rendering it insensitive to conformational changes induced by substrate binding. Notably, this conformational change could be substrate-dependent, with SAG potentially inducing a different conformational change than EnzChek lipase substrate. The detailed information about the allosteric binding pocket and the conformational changes induced by substrate binding remains unclear. Mutagenesis studies and affinity-based probes could help identify the structural features of DAGL enzymes.

In vitro and *in situ* ABPP studies of LEI-130 and LEI-131 confirmed their activity against DAGLβ with selectivity over a panel of serine hydrolases in mouse brain proteomes and living cells. Acute inhibition of DAGLβ by LEI-130 and LEI-131 resulted in decreased levels of 2-AG, AA, PGE_2 and PGD_2 in N9 microglia cells. However, this effect was not observed in J774A.1 macrophages. Interestingly, an increase of SAG, a substrate of DAGLβ, was observed in both cell lines treated with the inhibitors. These findings indicate that DAGLβ controls SAG levels in both cell lines, whereas the regulation of 2-AG levels is cell line-dependent. Besides being formed from phosphatidylinositol-4,5-bisphosphate (PIP_2) through the sequential actions of phospholipase C (PLC) and DAGL, 2-AG can also be generated from PIP_2 via an alternative pathway involving PIP_2 phosphatase, phospholipase A1 (PLA1) and lysophospholipase C (lysoPLC). This alternative pathway might be the dominant regulatory mechanism for 2-AG levels in J774A.1 macrophages. Although the inactive control LEI-132 showed no effects on the direct flux of 2-AG and SAG, it significantly influenced the production of other bioactive lipids in N9 microglia, likely by targeting DAGLβ-uncoupled pathways. Both DAGLβ active and inactive compounds attenuate LPS-stimulated cytokine productions, indicating that LPS might induce proinflammatory effects through DAGLβ-coupled and -uncoupled mechanisms.

In conclusion, the studies presented in this Chapter demonstrate that glycine sulfonamides LEI-130 and LEI-131 act as selective DAGLβ inhibitors and modulate inflammatory processes in immune cells. These compounds constitute a valuable chemical toolkit along with the control compound LEI-132 for studying the biological functions of DAGLβ. In the future, mass-spectrometry (MS)-based chemical proteomics could help reveal the potential off-targets of LEI-130, LEI-131 and LEI-132 that were not detected in gel-based ABPP.[28] Additionally, the absorption, distribution, metabolism and excretion (ADME) profile of these compounds should be determined prior to progressing to *in vivo* studies.

6.4 Acknowledgements

Wouter Driever is kindly acknowledged for evaluating the biochemical activity of the compounds against NAPE-PLD. Cas van der Horst is kindly acknowledged for evaluating the affinity of the compounds for cannabinoid CB_1 and CB_2 receptors. Mirjam Huizenga and Noëlle van Egmond are kindly acknowledged for their guidance in MAGL biochemical assay and ELISA, respectively. Max Louwerse is acknowledged for providing J774A.1 macrophages. Dr. Xinyu Di is kindly acknowledged for measuring lipid levels.

6.5 Experimental methods

Biology

Cell culture

N9 microglia cells were cultured at 37 °C under 7% CO_2 in Iscove's Modified Dulbecco's Medium (IMDM) containing phenol red, L-glutamine (2 mM), penicillin/streptomycin (200 µg/mL) and 5% sterile-filtered (0.2 µM) fatal calf serum (Thermo Fischer). J774A.1 macrophages were cultured at 37 °C under 5% CO_2 in Dulbecco′s modified Eagle′s medium (DMEM) containing phenol red, Glutamax (2 mM), penicillin/streptomycin (200 µg/mL) and 10% fatal calf serum (FCS, Thermo Fischer). Cells were passaged twice or three times a week by resuspension in fresh medium to appropriate confluence.

Total lysate preparation

Transient transfection was performed as described in Chapter 2. HEK293T cell pellets overexpressing human DAGLα and DAGLβ were thawed on ice and suspended in cold lysis buffer (20 mM HEPES pH 7.2, 250 mM sucrose, 2 mM DTT, 1 mM $MgCl_2$, 2.5 U/mL Benzonase). The suspension was pipetted up and down, incubated on ice for 30 min, and diluted in cold lysis buffer to 1 µg/µL. All samples were flash frozen in liquid N_2 and stored in small aliquots at -80 °C until use.

Preparation of mouse brain membrane and cytosol proteomes

Mouse brains were isolated according to guidelines approved by the ethical committee of Leiden University (AVD1060020171144), immediately flash frozen in liquid N_2 and stored at -80 °C until use. Upon preparation, mouse brains were thawed on ice and homogenized using a Wheaton™ Dounce homogenizer (3×7 sec) in cold lysis buffer (20 mM HEPES pH 7.2, 2 mM DTT, 1 mM $MgCl_2$, 25 U/mL Benzonase) and incubated on ice for 1 h. The lysate was spun at a low speed (2,500 g, 3 min, 4 °C, Eppendorf Centrifuge 5430R) to remove debris. Subsequently, the supernatant was subjected to ultracentrifugation (100,000 g, 45 min, 4 °C, Beckman Coulter, Ti 70.1 rotor) to obtain the membrane fraction as a pellet and the cytosolic fraction in the supernatant. The pellet was resuspended in cold storage buffer (20 mM HEPES pH 7.2, 2 mM DTT) and the total protein concentration was determined using Quick Start™ Bradford assay. The membrane and cytosol proteomes were diluted to 2 µg/µL, flash frozen in liquid N_2 and stored in small aliquots at -80 °C until use.

Activity-based protein profiling using probe DH379

Gel-based ABPP using DAGL-tailored probe DH379 was performed to determine the potency of the inhibitors for recombinant human DAGLβ and DAGLα. The total lysate of HEK293T cells overexpressing human DAGLα or DAGLβ (9.5 µL, 1 µg/µL) was incubated with DMSO or inhibitors at different concentrations (0.5 µL, 20× concentrated DMSO stocks) at rt for 30 min. DH379 (0.34 µL, 15 µM) was added and incubated for 10 min. The final concentration of

DH379 was 0.5 µM. Next, Laemmli blue (3.44 µL, 4× concentrated stock) was added and incubated for 10 min to quench the reaction. 10 µL of the quenched reaction mixture was resolved on 10% sodium dodecyl sulfate–polyacrylamide gel electrophoresis (SDS-PAGE) gels (180 V, 80 min) and the fluorescence was measured in a Biorad ChemiDoc™ MP system (Cy5: 700/50 filter; Cy3: 602/50 filter). The remaining enzymatic activity was determined based on the integrated fluorescent signal using Image Lab™ 6.0.0, which was corrected using the total protein loading per lane as determined by Coomassie stain (R250) and imaging (Coomassie Blue Gel: 590/110 filter). The pIC_{50} values were determined from the dose-response curves generated using GraphPad Prism 9.0.0 (log(inhibitor) vs. normalized response with variable slope). The assay was performed three times independently (n = 1, N = 3).

Michaelis-Menten kinetic assays

The membrane fraction of HEK293T cells overexpressing human DAGLα or DAGLβ was diluted in assay buffer (50 mM HEPES pH 7.5, 0.0025% Triton X-100) to 2 µg/mL. 1 µL of DMSO or inhibitors at different concentration (100× concentrated DMSO stocks) and 25 µL of protein solution were added to a black 96-well plate (Greiner Bio-One, REF 655076), followed by adding 70 µL assay buffer. After incubating at rt for 30 min, 4 µL of EnzChek at different concentrations (25× concentrated DMSO stocks, 8 concentrations) was added and the measurement was started immediately in CLARIOstar® (excitation 477-14 nm, emission 525-30 nm, gain = 1600, 72 sec/cycle for 61 cycles). The assay was performed in a final volume 100 µL with 0.5 µg/mL protein, different concentrations of inhibitors, different concentrations of EnzChek (0.05, 0.1, 0.2, 0.5, 0.8, 1, 1.5 and 2 µM), 5% DMSO and 0.0025% Triton X-100. The mock membrane fractions subjected to the same treatments were used for background measurements. The enzymatic rate (RFU/min) was determined from the slope between t = 6 min to t = 24 min after background subtraction, which was used to generate the Michaelis-Menten kinetic curves and Lineweaver Burk plots using GraphPad Prism 9.0.0 software. The assay was performed in n = 2, N = 2.

Activity-based protein profiling in mouse brain proteomes

Mouse brain membrane or cytosol proteome (19 µL, 2 µg/µL) was incubated with DMSO or compounds at different concentrations (0.5 µL, 40× concentrated DMSO stocks) at rt for 30 min. MB064 (0.5 µL, 40× concentrated DMSO stock) was added and incubated for 10 min. Subsequently, FP-BODIPY (0.5 µL, 40× concentrated DMSO stock) was added and incubated for another 10 min. Final concentration of probes MB064 and FP-BODIPY were 250 nM and 100 nM, respectively. Laemmli blue (7 µL, 4× concentrated stock) was added and incubated for 10 min to quench the reaction. 10 µL of the quenched reaction mixture was resolved on 10% SDS-PAGE gels (180 V, 80 min). Fluorescence and Coomassie were measured in a Biorad ChemiDocTM MP system (Cy5: 700/50 filter; Cy3: 602/50 filter; Cy2: 532/28 filter; Coomassie Blue Gel: 590/110 filter). The assay was performed twice independently (n = 1, N = 2).

Natural substrate-based fluorescent assay for human ABHD6 and MAGL

The natural substrate assay was performed in HEMNB buffer (50 mM HEPES pH 7.4, 1 mM EDTA, 5 mM $MgCl_2$, 100 mM NaCl, 0.5% (w/v) BSA) as previously reported.[27,29] 5 µL of DMSO or compounds at different concentrations (40× concentrated DMSO stocks) was incubated with 95 µL of the membrane fraction of HEK293T cells overexpressing human ABHD6 or MAGL diluted in HEMNB buffer (84 µg/mL for ABHD6, 3.2 µg/mL for MAGL) in a black 96-well plate (Greiner Bio-One, REF 655076) at rt for 30 min. The mock membrane fraction with DMSO was used for background measurement. Next, 100 µL of assay mix containing glycerol kinase (GK), glycerol-3-phosphate oxidase (GPO), horseradish peroxidase (HRP), adenosine triphosphate (ATP), Amplifu™Red and 2-arachidonoylglycerol (2-AG) was added and the measurement was started immediately at rt in CLARIOstar® (λ_{ex} = 535-20 nm, λ_{em} = 595-20 nm, 5 min/cycle for 13 cycles). The assay was performed in a final volume of 200 µL with 40 µg/mL protein for ABHD6, 1.5 µg/mL protein for MAGL, 0.2 U/mL GK, GPO and HRP, 0.125 mM ATP, 10 µM Amplifu™Red, 25 µM 2-AG, 5% DMSO, 1% ACN. The enzymatic rate was determined from the slope between t = 10 min to t = 35 min after background subtraction, which was normalized to generate the dose-dependent response curves using GraphPad Prism 9.0.0 (log(inhibitor) vs. normalized response with variable slope). All measurements were performed in n = 2, N = 2 or n = 4, N = 2 for controls, with Z' ≥ 0.6.

PED6 fluorescence assay for NAPE-PLD

The NAPE-PLD activity assay was performed as previously reported.[30]

Radioligand displacement assay for cannabinoid CB_1 and CB_2 receptors

The [^{3}H]CP55940 displacement assay was performed as previously reported.[31]

In situ target engagement and selectivity profiling

Target engagement 2.5×10^5 N9 microglia cells were seeded one day before the treatment in each well of a 6-well plate (Sarstedt, REF 83.3920). Before treatment, the medium was removed and the cells were washed once with PBS. The cells were treated with DMSO or compounds (1 µL, 10 mM) in 0.9 mL IMDM with 1% sterile-filtered FCS at 37 °C under 7% CO_2 for 1 h. Subsequently, DAGL-tailored probe DH379 (1 µL, 1 mM) in 0.1 mL of IMDM with 1% sterile-filtered FCS was added and the cells were incubated at 37 °C under 7% CO_2 for another 1 h. The final concentrations of compounds and probe DH379 were 10 µM and 1 µM, respectively. After this, the medium was removed and the cells were washed twice with cold PBS. 50 µL cold lysis buffer (20 mM HEPES pH 7.2, 250 mM sucrose, 1 mM $MgCl_2$ and 2.5 U/mL Benzonase) was added and the cells were lysed by scraping. The protein concentration was determined by Quick Start™ Bradford assay and all lysates were diluted to the same concentration (~1 µg/µL). For J774A.1 macrophage, 4×10^5 cells were seeded and incubated at 37 °C under 5% CO_2 and the treatment was done in DMEM with 1% FCS. 21 µL of lysate was incubated with 7 µL Laemmli blue (4× concentrated stock) for 10 min and 20 µL of the mixture

was resolved on 10% SDS-PAGE gels (180 V, 80 min). Fluorescence and Coomassie were measured in a Biorad ChemiDoc™ MP system (Cy5: 700/50 filter; Cy3: 602/50 filter; Coomassie Blue Gel: 590/110 filter). The assay was performed twice independently (n = 1, N = 2).

Selectivity profiling Cells were treated with DMSO or compounds (1 µL, 10 mM) in 1 mL medium with 1% corresponding serum at 37 °C for 2 h, followed by lysing through scraping. All lysates were diluted to the same concentration (~1 µg/µL). Subsequently, 19.5 µL of lysate was incubated with the cocktail of probes MB064 and FP-BODIPY (0.5 µL, 4 µM/each probe) at rt for 10 min. The final concentration of each probe was 100 nM. 6.7 µL Laemmli blue (4× concentrated stock) was then added and incubated for 10 min to quench the reaction. 20 µL of the quenched reaction mixture was resolved on 10% SDS-PAGE gels (180 V, 80 min). Fluorescence and Coomassie were measured in a Biorad ChemiDoc™ MP system (Cy5: 700/50 filter; Cy3: 602/50 filter; Cy2: 532/28 filter; Coomassie Blue Gel: 590/110 filter). The assay was performed twice independently (n = 1, N = 2).

Targeted lipidomics

Sample preparation 5×10^5 N9 microglia cells were seeded one day before the treatment in 6 cm dishes (Sarstedt, REF 83.3901). Before treatment, the medium was removed and the cells were washed once with PBS. The cells were treated with DMSO or compounds (final concentration 10 µM, 0.1% DMSO) in 3 mL IMDM with 1% sterile-filtered FCS at 37 °C under 7% CO_2 for 2 h. The treatment medium was removed and the cells were washed twice with cold PBS. 120 µL cold lysis buffer (20 mM HEPES pH 7.2, 250 mM sucrose, 1 mM $MgCl_2$ and 2.5 U/mL Benzonase) was added and the cells were lysed by scraping. The protein concentration was determined by Quick Start™ Bradford assay and 90 µL of lysate was stored in 1.5 mL Eppendorf safe-lock tubes at -80 °C until lipid extraction. For J774A.1 macrophage, 10^6 cells were seeded and incubated at 37 °C under 5% CO_2 and the treatment was done in DMEM with 1% FCS. The assay was performed in n = 5 for each condition.

Lipid extraction Lipid extraction was performed using liquid-liquid extraction under ice-cool conditions as previously reported.[32]

LC-MS/MS analysis Extracted samples were analyzed using two separate LCMS methods, Method 1 used a Shimadzu LC system (Shimadzu Corporation, Kyoto, Japan) connected to a SCIEX QTRAP 6500+ mass spectrometer (AB Sciex, Framingham, MA, USA). Separation was performed using a BEH C18 column (50 mm × 2.1 mm, 1.7 µm) from Waters Technologies (Mildford, MA, USA) maintained at 40 °C. The mobile phase was composed of 0.1% acetic acid in water (A), acetonitrile/0.1% acetic acid in methanol (90:10, v/v, B), and 0.1% acetic acid in isopropanol (C). The flow rate was set at 0.7 mL/min and the injection volume was 10 µL preceded by the injection of 20 µL of mobile phase A. Method 2 used a Shimadzu LC system (Shimadzu Corporation, Kyoto, Japan) connected to a SCIEX QTRAP 7500 mass spectrometer (AB Sciex, Framingham, MA, USA). Separation was performed using a BEH C8 column (50 mm × 2.1 mm, 1.7 µm) from Waters Technologies (Mildford, MA, USA)

maintained at 45 °C. The mobile phase was composed of 10 mM formic acid and 2 mM Ammonium formate in water (A), acetonitrile (B) and isopropanol (C). The flow rate was set at 0.4 mL/min and the injection volume was 5 µL preceded by the injection of 10 µL of mobile phase A. Ionization of the compounds in both methods was performed using electrospray ionization in negative mode. Selected Reaction Mode (SRM) was used for MS/MS acquisition. SRM transitions were individually optimized for targeted analytes and respective internal standards using standard solutions.

Data quality and data pre-processing For each target compound, the ratio between its peak area and the peak area of its respective internal standard was calculated using SCIEX OS-MQ Software and used for further data analysis. The quality of the data was monitored using regular injection of quality control (QC) samples, consisting of blank samples, within the sequence. QC samples were used to correct for inter-batch variations using the in-house developed mzQuality workflow (available at http://www.mzQuality.nl). Relative standard deviations (RSDs) of peak area ratios were calculated for each targeted analyte detected in the QC samples.

Enzyme-linked immunosorbent assay (ELISA)

***In situ* treatment** 2×10^4 N9 cells were seeded one day before the treatment in the wells of a 96-well plate (Sarstedt, REF 83.3924) and incubated at 37 °C under 7% CO_2. Before treatment, the medium in the inner wells was removed and the cells were washed once with PBS. The cells were treated with DMSO or compounds in 70 µL IMDM with 1% sterile-filtered FCS at 37 °C under 7% CO_2 for 1 h. Subsequently, LPS in 30 µL of IMDM with 1% sterile-filtered FCS was added and the cells was incubated at 37°C under 7% CO_2 for 24 h. The final concentrations of compounds and LPS were 10 µM and 5 ng/mL, respectively. The treatment supernatant was collected for ELISA. The cells were incubated with Alamar Blue (3 mM) in IMDM with 5% sterile-filtered FCS for 4 h to check the cell viability. For J774A.1 macrophage, 2×10^4 cells were seeded and incubated at 37 °C under 5% CO_2. The treatment was done in DMEM with 1% FCS and cell viability was assessed by Alamar Blue (3 mM) in DMEM with 10% FCS. The assay was performed in n = 4, N = 4 for each condition.

ELISA Enzyme-linked immunosorbent assay (ELISA) was performed using Invitrogen IL-6 Mouse uncoated ELISA kit (cat 88-7064-88) and TNF alpha Mouse uncoated ELISA kit (cat 88-7324-88) following the protocol from the manufacture with modifications. In brief, half area high binding 96-well plates (Greiner Bio-One, REF 675061) were coated with 25 µL of capture antibody in PBS (1:250) overnight at 4 °C. The plate was washed three times with PBST (1×PBS with 0.05% tween-20) and then blocked with 100 µL of ELISPOT (1×) at rt for 1 h. After another three washes with PBST, 25 µL of treatment supernatant or standard solutions were added and incubated for 2 h. The plate was washed three times and 25 µL of the biotinylated detection antibody (1:250) diluted in ELISPOT was added and incubated for 1 h. Subsequently, the plate was washed three times with PBST and 25 µL of the enzyme Streptavidin-HRP (1:100) diluted in ELISPOT was added and incubated for 30 min. The plate was washed seven times with PBST. Detection was performed by reacting with 25 µL of TMB solution for around 10 min, followed by quenching with 10 µL of 1 M aqueous HCl solution.

Absorbance was measured at 450 nm and 570 nm in CLARIOstar® and 570 nM values were subtracted from 450 nm values to correct for background. The calibration curve was fitted by a 4P-sigmoidal curve in GraphPad Prism 9.0.0, with logarithmically transformed concentrations plotted against the corrected absorbance values.

Chemistry

General remarks

All purchased chemicals were used without purification unless stated otherwise. All reactions were performed in oven-dried or flame-dried glassware. Anhydrous solvents were dried by activated 3 Å or 4 Å molecular sieves. Thin layer chromatography (TLC) analysis was performed on Merck silica gel 60 F_{254} aluminium sheets and the compounds were visualized by using UV absorption at 254 nm and/or $KMnO_4$ staining (5 g/L $KMnO_4$ and 25 g/L K_2CO_3 in water). TLC plates were analysed with the Advion CMS Plate Express® connected to the Advion Expression® L-MS using 90% MeOH in H_2O with 0.1% formic acid as the solvent. Purification was performed on automated silica gel column chromatography (40-63 µm, 60 Å pre-packed silica gel, Screening Devices) on a Biotage Isolera™ Four 3.0 system. ^1H and ^{13}C spectra were recorded on AV 400 MHz spectrometer (400 MHz for ^1H and 101 MHz for ^{13}C) in deuterated solvents. Chemical shifts are reported in ppm with tetramethylsilane (TMS) or solvent resonance as the internal standard ($CDCl_3$: δ 7.26 for ^1H, δ 77.16 for ^{13}C; CD_3OD: δ 3.31 for ^1H, 49.00 for ^{13}C). Data is reported as follows: chemical shifts δ (ppm), multiplicity (s = singlet, d = doublet, dd = doublet of doublets, t = triplet, quintet = p, m = multiplet), coupling constants *J* (Hz) and integration. High resolution mass spectrometry (HRMS) analysis was performed on a Thermo Finnigin LTQ Orbitrap mass spectrometer equipped with an electrospray ion source in positive mode (source voltage 3.5 kV, sheath gas flow 10 mL/min, capillary temperature 250 °C) with resolution R = 60000 at m/z 400 (mass range m/z = 150-2000) and dioctyl phthalate (m/z = 391.28428) as a lock mass.

4-((*N*-(1-(3-Chloro-4-(trifluoromethyl)phenyl)cyclobutyl)-3,4-dihydro-2*H*-benzo[*b*][1,4]diozepine)-7-sulfonamido)butanoic acid (7, LEI-132)

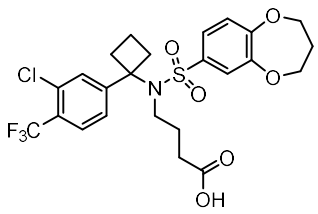

To a solution of methyl 4-((*N*-(1-(3-chloro-4-(trifluoromethyl)phenyl)cyclobutyl)-3,4-dihydro-2*H*-benzo[*b*][1,4]dioxepine)-7-sulfonamido)butanoate (**8**, 42 mg, 0.075 mmol, 1 eq) in THF/MeOH (0.75 mL/0.75 mL, 0.05 M) was added 1 M aq. LiOH (0.3 mL, 0.3 mmol, 4 eq). The mixture was stirred at rt for overnight. The reaction mixture was diluted in 0.1 M aq. HCl and extracted 3× with EtOAc. The combined organic layers were washed with brine, dried over anhydrous Na_2SO_4, filtered and concentrated. The residue was purified by silica gel column chromatography (0-3% MeOH in DCM) to afford the product (36 mg, 0.066 mmol, 87%). ^1H NMR (400 MHz, MeOD+$CDCl_3$) δ 7.62 (d, *J* = 8.1 Hz, 1H), 7.56 – 7.47 (m, 2H), 7.00 (dd, *J* = 8.5, 2.4 Hz, 1H), 6.89 (d, *J* = 2.3 Hz, 1H), 6.84 (d, *J* = 8.5 Hz, 1H), 4.26 (t, *J* = 5.7 Hz, 2H), 4.20 (t, *J* = 5.8 Hz,

2H), 3.31 (t, J = 7.2 Hz, 2H), 2.83 – 2.69 (m, 2H), 2.59 – 2.48 (m, 2H), 2.28 (t, J = 6.9 Hz, 2H), 2.19 (p, J = 5.8 Hz, 2H), 1.93 (p, J = 7.1 Hz, 2H), 1.85 – 1.75 (m, 1H), 1.68 – 1.53 (m, 1H). ^{13}C NMR (101 MHz, MeOD+$CDCl_3$) δ 175.79, 155.07, 151.13, 149.91, 135.50, 132.65 (q, $J_{C\text{-}F}$ = 1.9 Hz), 130.75, 127.94 (q, $J_{C\text{-}F}$ = 5.3 Hz), 127.68 (q, $J_{C\text{-}F}$ = 31.9 Hz), 125.80, 123.40 (q, $J_{C\text{-}F}$ = 273.2 Hz), 122.66, 121.99, 120.81, 71.06, 70.88, 65.72, 47.53, 35.75, 31.50, 31.32, 27.22, 14.83. HRMS $[C_{24}H_{25}ClF_3NO_6S+Na]^+$: 570.09354 calculated, 570.09435 found.

Methyl 4-((*N*-(1-(3-chloro-4-(trifluoromethyl)phenyl)cyclobutyl)-3,4-dihydro-2*H*-benzo[*b*][1,4]dioxepine)-7-sulfonamido)butanoate (8)

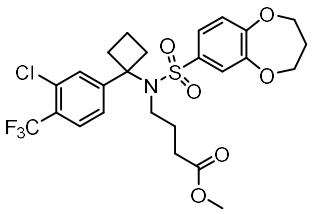

To a solution of *N*-(1-(3-chloro-4-(trifluoromethyl)phenyl)cyclobutyl)-3,4-dihydro-2*H*-benzo[*b*][1,4]dioxepine-7-sulfonamide (54.0 mg, 0.117 mmol, 1 eq) in anhydrous DMF (1.2 mL, 0.1 M) was added methyl 4-bromobutanoate (29.6 µL, 0.234 mmol, 2 eq) and BEMP (1 M in hexane, 234 µL, 0.234 mmol, 2 eq). The mixture was heated at 80 °C for overnight. The reaction mixture was diluted in 0.1 M aq. HCl and extracted 3× with EtOAc. The combined organic layers were washed with brine, dried over anhydrous Na_2SO_4, filtered and concentrated. The residue was purified by silica gel column chromatography (15-25% EtOAc in *n*-pentane) to afford the product (51 mg, 0.091 mmol, 78%). ^{1}H NMR (400 MHz, $CDCl_3$) δ 7.62 (d, J = 8.2 Hz, 1H), 7.56 – 7.51 (m, 1H), 7.50 (d, J = 1.8 Hz, 1H), 7.03 (dd, J = 8.4, 2.4 Hz, 1H), 6.97 (d, J = 2.3 Hz, 1H), 6.85 (d, J = 8.4 Hz, 1H), 4.29 (t, J = 5.8 Hz, 2H), 4.23 (t, J = 5.9 Hz, 2H), 3.68 (s, 3H), 3.33 – 3.26 (m, 2H), 2.83 – 2.71 (m, 2H), 2.60 – 2.50 (m, 2H), 2.31 (t, J = 6.9 Hz, 2H), 2.22 (p, J = 5.8 Hz, 2H), 2.01 – 1.91 (m, 2H), 1.87 – 1.77 (m, 1H), 1.69 – 1.59 (m, 1H). ^{13}C NMR (101 MHz, $CDCl_3$) δ 173.44, 154.39, 150.58, 149.44, 135.47, 132.33 (q, $J_{C\text{-}F}$ = 2.0 Hz), 130.21, 127.55 (q, $J_{C\text{-}F}$ = 5.0 Hz), 127.32 (q, $J_{C\text{-}F}$ = 31.5 Hz), 125.35, 122.91 (q, $J_{C\text{-}F}$ = 269.8 Hz), 122.24, 121.51, 120.47, 70.53, 70.37, 65.17, 51.86, 47.06, 35.30, 31.10, 30.90, 26.65, 14.57.

References

1. Mechoulam, R. *et al.* Identification of an endogenous 2-monoglyceride, present in canine gut, that binds to cannabinoid receptors. *Biochem. Pharmacol.* **50**, 83–90 (1995).
2. Devane, W. A. *et al.* Isolation and structure of a brain constituent that binds to the cannabinoid receptor. *Science* **258**, 1946–1949 (1992).
3. Busquets-García, A., Bolaños, J. P. & Marsicano, G. Metabolic Messengers: endocannabinoids. *Nat. Metab.* **4**, 848–855 (2022).
4. Castillo, P. E., Younts, T. J., Chávez, A. E. & Hashimotodani, Y. Endocannabinoid Signaling and Synaptic Function. *Neuron* **76**, 70–81 (2012).
5. Mackay, H. J. & Twelves, C. J. Targeting the protein kinase C family: Are we there yet? *Nat. Rev. Cancer.* **7**, 554–562 (2007).
6. Boyce, J. A. Mast cells and eicosanoid mediators: A system of reciprocal paracrine and autocrine regulation. *Immunol. Rev.* **217**, 168–185 (2007).
7. Papackova, Z. & Cahova, M. Fatty acid signaling: The new function of intracellular lipases. *Int. J. Mol. Sci.* **16**, 3831–3855 (2015).
8. Alger, B. E. & Kim, J. Supply and demand for endocannabinoids. *Trends Neurosci.* **34**, 304–315 (2011).
9. Bisogno, T. *et al.* Cloning of the first sn1-DAG lipases points to the spatial and temporal regulation of endocannabinoid signaling in the brain. *J. Cell Biol.* **163**, 463–468 (2003).
10. Karlsson, M., Contreras, J. A., Hellman, U., Tornqvist, H. & Holm, C. cDNA cloning, tissue distribution, and identification of the catalytic triad of monoglyceride lipase. Evolutionary relationship to esterases, lysophospholipases, and haloperoxidases. *J. Biol. Chem.* **272**, 27218–27223 (1997).
11. Blankman, J. L., Simon, G. M. & Cravatt, B. F. A Comprehensive Profile of Brain Enzymes that Hydrolyze the Endocannabinoid 2-Arachidonoylglycerol. *Chem. Biol.* **14**, 1347–1356 (2007).
12. Griner, E. M. & Kazanietz, M. G. Protein kinase C and other diacylglycerol effectors in cancer. *Nat. Rev. Cancer* **7**, 281–294 (2007).
13. Kolczynska, K., Loza-Valdes, A., Hawro, I. & Sumara, G. Diacylglycerol-evoked activation of PKC and PKD isoforms in regulation of glucose and lipid metabolism: A review. *Lipids Health Dis.* **19**, 1–15 (2020).
14. Rouzer, C. A. & Marnett, L. J. Endocannabinoid oxygenation by cyclooxygenases, lipoxygenases, and cytochromes P450: Cross-talk between the eicosanoid and endocannabinoid signaling pathways. *Chem. Rev.* **111**, 5899–5921 (2011).
15. Samovski, D., Jacome-Sosa, M. & Abumrad, N. A. Fatty Acid Transport and Signaling: Mechanisms and Physiological Implications. *Annu. Rev. Physiol.* **85**, 317–337 (2023).
16. Cooke, M. & Kazanietz, M. G. Overarching roles of diacylglycerol signaling in cancer development and antitumor immunity. *Sci. Signal.* **15**, 1–27 (2022).

17. Nomura, D. K. *et al.* Endocannabinoid hydrolysis generates brain prostaglandins that promote neuroinflammation. *Science* **334**, 809–813 (2011).

18. Gao, Y. *et al.* Loss of retrograde endocannabinoid signaling and reduced adult neurogenesis in diacylglycerol lipase knock-out mice. *J. Neurosci.* **30**, 2017–2024 (2010).

19. Tanimura, A. *et al.* The Endocannabinoid 2-Arachidonoylglycerol Produced by Diacylglycerol Lipase α Mediates Retrograde Suppression of Synaptic Transmission. *Neuron* **65**, 320–327 (2010).

20. Viader, A. *et al.* A chemical proteomic atlas of brain serine hydrolases identifies cell type-specific pathways regulating neuroinflammation. *Elife* **5**, 1–24 (2016).

21. Berger, N. *et al.* Inhibition of diacylglycerol lipase β modulates lipid and endocannabinoid levels in the ex vivo human placenta. *Front. Endocrinol.* **14**, 1–12 (2023).

22. Hsu, K.-L. *et al.* DAGLβ inhibition perturbs a lipid network involved in macrophage inflammatory responses. *Nat. Chem. Biol.* **8**, 999–1007 (2012).

23. Ogasawara, D. *et al.* Rapid and profound rewiring of brain lipid signaling networks by acute diacylglycerol lipase inhibition. *Proc. Natl. Acad. Sci. U.S.A.* **113**, 26–33 (2016).

24. Jenniches, I. *et al.* Anxiety, Stress, and Fear Response in Mice with Reduced Endocannabinoid Levels. *Biol. Psychiatry* **79**, 858–868 (2016).

25. Cavener, V. S. *et al.* Inhibition of Diacylglycerol Lipase Impairs Fear Extinction in Mice. *Front. Neurosci.* **12**, 1–10 (2018).

26. Baggelaar, M. P. *et al.* Development of an Activity-Based Probe and In Silico Design Reveal Highly Selective Inhibitors for Diacylglycerol Lipase-α in Brain. *Angew. Chem. Int. Ed.* **52**, 12081–5 (2013).

27. Janssen, F. J. *et al.* Discovery of Glycine Sulfonamides as Dual Inhibitors of sn -1-Diacylglycerol Lipase α and α/β-Hydrolase Domain 6. *J. Med. Chem.* **57**, 6610–6622 (2014).

28. Porta, E. O. J. & Steel, P. G. Activity-based protein profiling: A graphical review. *Curr. Res. Pharmacol. Drug Discov.* **5**, 100164 (2023).

29. Navia-Paldanius, D., Savinainen, J. R. & Laitinen, J. T. Biochemical and pharmacological characterization of human α/β-hydrolase domain containing 6 (ABHD6) and 12 (ABHD12). *J. Lipid Res.* **53**, 2413–2424 (2012).

30. Mock, E. D. *et al.* Discovery of a NAPE-PLD inhibitor that modulates emotional behavior in mice. *Nat. Chem. Biol.* **16**, 667–675 (2020).

31. Soethoudt, M. *et al.* Cannabinoid CB2 receptor ligand profiling reveals biased signalling and off-target activity. *Nat. Commun.* **8**, (2017).

32. Di Zazzo, A. *et al.* Signaling lipids as diagnostic biomarkers for ocular surface cicatrizing conjunctivitis. *J. Mol. Med.* **98**, 751–760 (2020).

Supplementary Figures and Tables

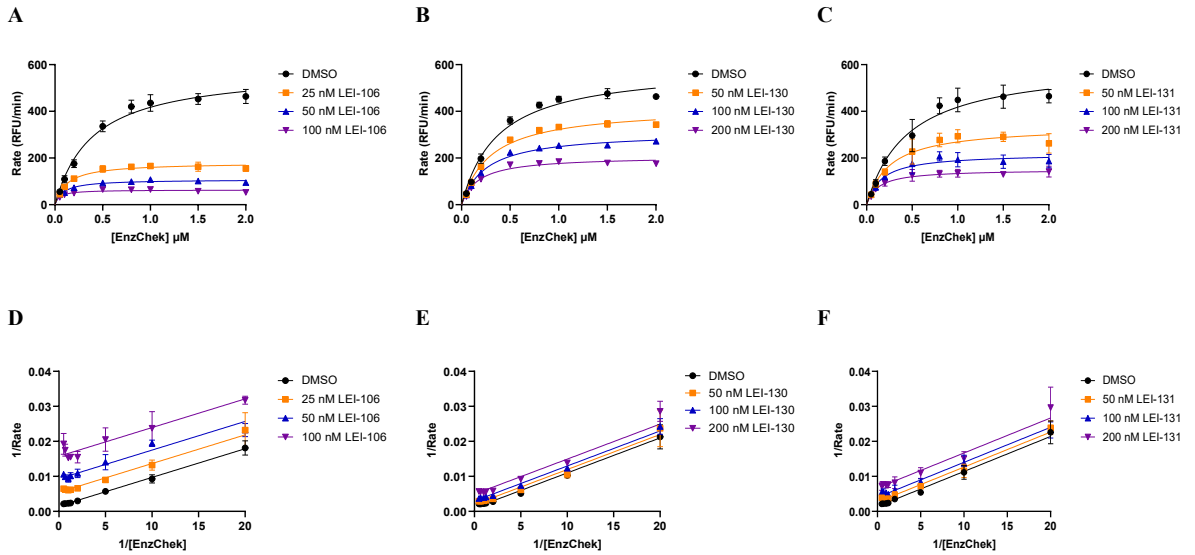

Supplementary Figure S6.1 Mode-of-inhibition studies of LEI-106, LEI-130 and LEI-131 against DAGLα. (A-C) Michaelis-Menten kinetic curves. Rate of EnzChek hydrolysis by DAGLα as a function of substrate concentration in the presence of different concentrations of LEI-106, LEI-130 and LEI-131. (D-F) Lineweaver Burk plots. Data shown are mean ± SD (n = 2, N = 2).

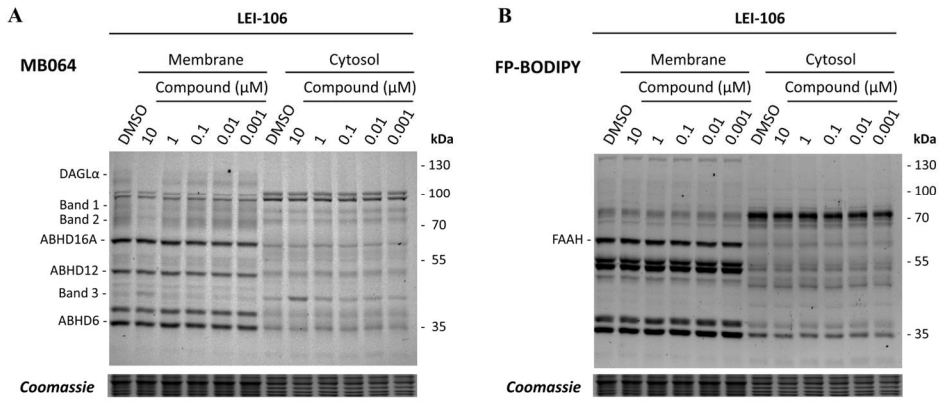

Supplementary Figure S6.2 *In vitro* selectivity of LEI-106 on mouse brain proteomes. Representative gels of ABPP experiments using MB064 (A, 250 nM, 10 min) and subsequently FP-BODIPY (B, 100 nM, 10 min).

Supplementary Table S6.1 Summary of V_{max} and K_M values for DAGLβ in the presence of different concentrations of LEI-106, LEI-130 and LEI-131.

Compound	Concentration (nM)	V_{max} (RFU/min)	K_M (µM)
LEI-106	0	176 ± 11	0.26 ± 0.07
	25	124 ± 11	0.28 ± 0.07
	50	90 ± 7	0.20 ± 0.05
	100	72 ± 10	0.23 ± 0.11
LEI-130	0	165 ± 12	0.31 ± 0.08
	5	102 ± 8	0.29 ± 0.08
	10	74 ± 6	0.28 ± 0.08
	20	60 ± 10	0.31 ± 0.12
LEI-131	0	195 ± 14	0.29 ± 0.07
	5	89 ± 9	0.27 ± 0.11
	10	54 ± 5	0.24 ± 0.10
	20	38 ± 5	0.24 ± 0.09

Supplementary Table S6.2 Summary of V_{max} and K_M values for DAGLα in the presence of different concentrations of LEI-106, LEI-130 and LEI-131.

Compound	Concentration (nM)	V_{max} (RFU/min)	K_M (µM)
LEI-106	0	581 ± 39	0.39 ± 0.07
	25	180 ± 9	0.13 ± 0.03
	50	108 ± 6	0.09 ± 0.02
	100	63 ± 5	0.05 ± 0.02
LEI-130	0	593 ± 35	0.37 ± 0.07
	50	418 ± 19	0.30 ± 0.04
	100	311 ± 11	0.25 ± 0.03
	200	207 ± 9	0.17 ± 0.03
LEI-131	0	607 ± 57	0.45 ± 0.12
	50	337 ± 35	0.25 ± 0.07
	100	219 ± 22	0.16 ± 0.05
	200	151 ± 11	0.13 ± 0.04